Arbitrary black-string deformations in the black string-black hole transitions

Matthew Anderson[1,2], Luis Lehner[1], Jorge Pullin[1,2]
1 *Department of Physics and Astronomy, Louisiana State University, Baton Rouge, LA 70803-4001*
2 *Center for Computation and Technology, Louisiana State University, Baton Rouge, LA 70803-4001*

We study the possible black string-black hole transition by analyzing the structure of the apparent horizon for a large family of time-symmetric initial data. We observe that, as judged by the apparent horizon, it is possible to generate arbitrarily deformed black strings at a moment of time symmetry. A similar study for hyperspherical black holes reveals that although arbitrarily deformed hyperspherical black holes can be constructed, the proper distance between the north and south poles along the extra direction has an upper limit.

I. INTRODUCTION

The dynamics of black strings has been the subject of significant attention in recent years and several results have appeared in the literature indicating the evolution of a sufficiently long perturbed blackstring is likely richer than anticipated. Considerable interest was initially sparked when Gregory and Laflamme [1, 2], noted that in linearized perturbation theory black strings longer than a certain length become unstable. The work of Horowitz and Maeda shows that if the spacetime continues to be asymptotically predictable, black strings cannot pinch-off in finite affine time [3] and also presents additional arguments against the pinch-off possibility in lieu of the perturbed string evolving towards a stationary non-uniform string. This suggestion has spurred several papers —and conjectures— about what fate a perturbed string might encounter (see for instance [3, 4, 5]).

However, there is not yet agreement on what the final fate might be and different analyses are being carried out to shed light on this issue. For instance, stationary solutions which are non-uniform in the extra dimension have been obtained [6, 7] but their entropy (for dimensions lower than 14 [8]) is too large for these solutions to be the end point of the dynamical evolution envisaged by Horowitz and Maeda[6, 7]. Further analysis of highly distorted stationary strings have revealed the spacetime around the neck approaches one having a conical structure. It is therefore conjectured that a perturbed string can pinch-off discontinuously, experiencing a conical phase[9, 10].

Numerical simulations have also been presented which reveal the rich dynamics of a perturbed black string, where the initially exponentially fast varying geometry characterizing the (highly distorted) horizon neighborhood gives rise to a later stage where the dynamics are significantly slowed down [11]. Although lack of resolution prevented pushing the simulation further, a study of the late stages of the solution indicated that the possibility of the horizon pinching off in infinite affine time is quite possible [12]. Extrapolating the observed results further, the pinching off, if it happens, could proceed in a smooth way. Though this possibility, as well as all other conjectures, awaits for numerical evolutions for a definitive statement.

There is still much to be understood before a clear picture of the problem emerges. It turns out interesting information can be extracted by considering a sequence of initial data which aims to probe a region close to a bifurcation scenario. This line of work has been previously pursued by Sorkin and Piran [13] inspired by related work in the study of binary black hole collisions. At the core of the idea is to find particular solutions at a given instant of time (thus satisfying the constraint equations) which describe a highly distorted black string (as judged by their apparent horizons) and examine what occurs as this distortion is made more extreme. The constraints are solved in the presence of a matter source with at least one free parameter characterizing its size. By varying this parameter, one can find hyperspherical black holes —when the source is sufficiently compact and localized— or black strings —when the source is compact but distributed along the extra dimension. By fine-tuning this parameter one can thus study what type of transition is observed in highly distorted cases. To simplify the task of finding consistent data in the presence of this source a moment of time symmetry can be chosen, and so the momentum constraint is trivially satisfied. The solution of the Hamiltonian constraint yields the data sought after. Once this is found, an analysis of the apparent horizon at that hypersurface gives an indication of what the behavior may be. Unfortunately, this approach cannot give the event horizon behavior, but since it must contain the apparent horizon, the latter does give some indication of how the former behaves.

In the present work we study the problem and obtain numerical solutions for a variety of sources which are chosen to probe deeply the transition region between black holes and strings. We consider a D dimensional spacetime endowed with a $SO(D-2)$ symmetry and develop a code able to yield solutions of the initial data problem for Einstein's equations at a moment of time symmetry in the presence of an arbitrary chosen source. This allows us to probe a family of solutions interpolating between hyperspherical black holes and black strings. To do so, we examine

a sequence of solutions describing distorted black holes and strings and study their properties. We define such a sequence by varying the source while keeping the two relevant scales in the problem —namely the ADM mass per unit length of the spacetime and the asymptotic length of the extra dimension— constant. This fact, coupled to the ability of examining arbitrary spherical dimensions and the use of computational techniques that let us probe significantly distorted strings are the main differences with the work presented in [13]. As we will see, our results agree with most of those presented there, but also interesting differences arise. Most importantly, we are able to produce arbitrarily distorted strings by appropriately varying the source considered. By analyzing these strings, we find features common to the solutions found in simulations of perturbed black strings which could explain the slow down of the dynamics observed there [11].

II. PROBLEM SET UP

The analysis of allowed solutions in arbitrary dimensions has recently revealed a possible interesting behavior at large enough dimensions [14, 15] through a linearized analysis of the solution's behavior. Indeed these results would indicate in dimensions > 13 the conjecture of Horowitz–Maeda, namely that a perturbed string might settle down to a non-uniform stationary string, is quite more plausible than in lower dimensional cases. This is hinted by the behavior of thermodynamical quantities which revealed the transition from a uniform string to a distorted one is continuous for high enough dimensions.

It is thus interesting to consider finding solutions for arbitrary dimensions and examine the possible differences that may arise. If this marked transition at sufficiently high dimensions is robust beyond the linear regime, its effects would likely be evident in the solutions obtained. However, obtaining such solutions in large dimensions is a delicate enterprise since fields near the origin acquire a much steeper gradient. Furthermore, if one is interested in constructing highly distorted situations —in particular to discern the behavior at a threshold of a very thin string— numerical techniques capable of probing these scenarios must be employed. We thus adopt the following strategy to construct a code capable of dealing with these issues.

We begin by extending the same approach followed in [13]. We consider time-symmetric, space-like hypersurfaces and choose a conformally flat metric for simplicity:

$$dl^2 = \psi^2 \left(dr^2 + dz^2 + r^2 d\Omega_{D-3}^2 \right), \tag{1}$$

where D is the dimension of a spacetime with $SO(D-2)$ symmetry. While the momentum constraint is trivially satisfied, the Hamiltonian constraint becomes

$$\partial_{rr}\psi + \partial_{zz}\psi + \frac{(D-3)}{r}\partial_r\psi + \left[(\partial_r\psi)^2 + (\partial_z\psi)^2 \right] \left[\frac{(D-4)(D-3)}{2} - 1 \right] / (D-2) + \rho\psi^3 = 0. \tag{2}$$

Following the arguments given in [16], a well posed problem to solve for ψ from Eq. 2 can be obtained if the matter density is rescaled as $\rho \to \tilde{\rho}\psi^{-3-s}$.

We solve the resulting equation with the use of finite element techniques. This enables a smooth mesh grading to support higher resolution near the matter density. Converting Eq. 2 into the weak form for finite element simulation also conveniently removes the coordinate singularity at $r = 0$. Simulations used bilinear quadrilateral elements with full approximation scheme (FAS) multigrid as the solver [17]. We used the Diffpack finite element toolkit [18] in all development and production runs.

In the present paper we concentrate on the $D = 5$ case both for testing purposes and to re-examine the results in [13] with a well defined sequence that keeps both the ADM mass and the asymptotic length of the extra dimension fixed. We do so by appropriately varying the source. The results for higher dimensions will be presented elsewhere.

In five dimensions, Eq. 2 becomes

$$\frac{1}{r^2}\partial_r \left(r^2 \partial_r \right) \psi + \partial_{zz}\psi + \tilde{\rho}\psi^{-s} = 0. \tag{3}$$

We chose $s = 1$ for all simulations in the present case. The non-physical density $\tilde{\rho}$ was chosen to be

$$\tilde{\rho} = A \exp\left(-r^2/\sigma_r^2\right) \left[\exp\left(-z^2/\sigma_z^2\right) + \exp\left(-\left(z - 2L\right)^2/\sigma_z^2 \right) \right] + A \exp\left(-r^2/\sigma_A^2\right) \exp\left(-z^2/\sigma_B^2\right), \tag{4}$$

with $\sigma_r = 0.1$, $\sigma_z = 0.1$, and $\sigma_A \in [0.025, 1.0]$ and $\sigma_B \in [0.1, 2.0]$. The first term of this source is also identical to reference [13]. The second term of the source is intended to increase the distortion of the black object horizon by increasing the matter density in the periodic direction close to $r = 0$.

In our sequence of solutions, the amplitude, A was varied to ensure the ADM mass remained the same for all density distributions. The size of the periodic dimension, $2L$, was chosen identical to reference [13] ($L = 2$) and longer ($L = 15$) so as to cover cases above and below Gregory–Laflamme's critical length. The adopted boundary conditions are as those in [13]: reflection symmetries, $\partial_r \psi = 0$ along $r = 0$ and $\partial_z \psi = 0$ along $z = 0$; periodicity, $\partial_z \psi = 0$ along $z = L$; and Robin, $\partial_r (r\psi) = 1$, at the r outer boundary. The last condition ensures the asymptotic length of the extra dimension is constant. All our simulations have been carried out for different locations of the outer boundary given by $r = 5, 10, 20, 50$ without observing significant differences in the obtained solution.

Variations in the non-physical density distribution can produce either black strings or hyperspherical black holes. Locating the apparent horizon indicates the type of black object present in the initial data. The apparent horizon is the outermost surface of zero-expansion of null rays. For initial data with vanishing extrinsic curvature, the apparent horizon satisfies

$$\nabla_i s^i = 0, \tag{5}$$

where s^i are the spatial indices of the space-like normal to the horizon surface. For black string solutions, we consider the function $\phi = r - \rho(z)$ and find the surface where $\phi = 0$ by solving Eq. 5. For black hole solutions, we transform to spherical coordinates R, χ where $r = R\sin(\chi)$ and $z = R\cos(\chi)$, following the approach described in [15]. We then consider the function $\phi = R - \rho(\chi)$ and locate the surface where $\phi = 0$.

III. RESULTS

The code was tested using an independent residual evaluator. Additionally, it was tested by recovering uniform black string and hyperspherical black hole solutions. Further tests were conducted comparing cases using two entirely different finite element toolkits, FlexPDE [19] and Diffpack [18]. The tests cases employed adaptive triangular meshes in the FlexPDE toolkit and graded quadrilateral meshes in the Diffpack toolkit, with excellent agreement. In all cases, good convergence of the solution was observed. For instance, Figure 1 shows the error as reported by the independent residual evaluator for a uniform black string along the radius at $z = 1$ at three resolutions. The convergence in the L2 norm is slightly better than first order. As expected, the absolute error is larger near the artificial matter distribution. A sense of the relative error with respect to the defined source is given by monitoring the error divided by $\tilde{\rho} + 1$. All results apart from the convergence tests used resolutions of $dr = 0.00225$ and $dz = 0.002$, unless otherwise noted.

After validating the code, we proceeded to study both distorted strings and hyperspherical black holes.

We first considered the behavior of distorted hyperspherical black holes. Using the source given by Eq. 4, we fix both σ_r and σ_z to be 0.1. This choice would produce a uniform hyperspherical black hole if the second term of Eq. 4 were absent. We employ this second term to generate sequences of initial data by using increasingly larger σ_B values which produce more distorted black holes until a black string horizon results, holding σ_A constant. Four classes of data are generated, each with a particular value for σ_A. The smaller the σ_A choice is, the more distorted the resulting horizon will appear. See Figure 2.

A useful quantity to monitor whether a black hole can be distorted so as to approach a black string is to consider the proper length between the two poles, as done in [13]. We thus evaluate this quantity by considering

$$l = \int_{r^{(5)}}^{L} \psi\,(r = 0, z)\, dz. \tag{6}$$

For each of the four sequences of initial data, all approach ~ 1.8 even though the initial data generated using the smallest σ_A choices produced more distorted black holes than the largest choices. The deformation of the hole, λ', is given by

$$\lambda' = \frac{R^{(5)}_{\max}}{R^{(5)}_{\min}} - 1, \tag{7}$$

with $R_{\max}, R_{\min}$ the proper distance along the z and r axis. The results for l for different cases are shown in Figure 3. Clearly, as indicated by the apparent horizon, there does seem to be an upper limit as to how close the poles can be even when black hole horizons could be found to be more distorted. This would indicate that the spacetime in between the poles is becoming considerably curved.

We now turn our attention to a family of gradually more distorted black strings. The distortion of a black string, λ, is given by

$$\lambda = \frac{1}{2}\left(\frac{r^{(4)}_{\max}}{r^{(4)}_{\min}} - 1\right), \tag{8}$$

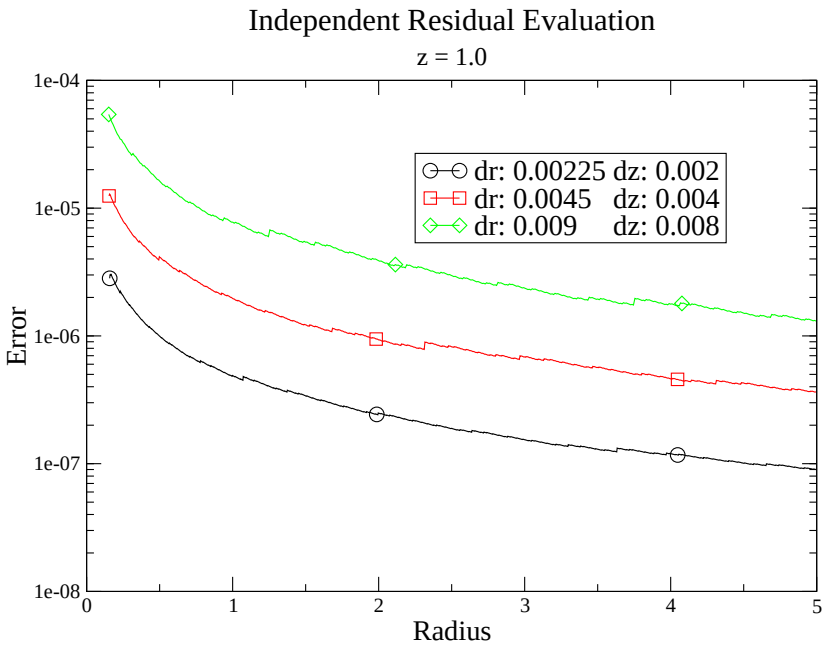

FIG. 1: The unscaled error for a uniform black string along the radius at $z = 1$ at three resolutions. For the highest resolution at $r = 0.01$, the error scaled by $\tilde{\rho} + 1$ was 1.3×10^{-5}; $\tilde{\rho}$ was 3.48×10^{5}.

where $r_{\rm max}, r_{\rm min}$ are the maximum/minimum areal radius of the apparent horizon. We fix $\sigma_r = \sigma_z = 0.1$ and vary σ_A and σ_B; this gives rise to black string solutions with large degree of distortions (see Figure 4). Indeed, we have found distortions up to $\lambda \simeq 5$ without anything to prevent obtaining even larger distortions (apart from discretization issues). To make this more evident Figure 5 illustrates what the distortion λ vs σ_B is for three different values of σ_A (Recall that σ_A, σ_B govern the source's deformation along r,z directions). The same behavior is evident when the periodic dimension is larger than the Gregory–Laflamme critical length (see Fig. 7).

Finally, we examine the Kretschmann invariant K value for different members of the sequence, in particular we consider the quantity $I = KR_{ah}^4/12$ which, as mentioned in [11], would give a value of 6 for a uniform hyperspherical black hole while 1 for a uniform stationary black string. Interestingly, near the origin, the value of this invariant is close to 6 while relatively close to 1 at $z \simeq 1$. Furthermore, the region in between behaves in a way quite similar to that found at the late stages of the evolution in [11]. This could indicate that the slow down observed there might be a result of the dynamical solution approaching a time symmetric phase. If this were the case it would give support to the conjecture that a "breathing" scenario might take place [20]. In this picture the deformed black string would reach a stage where the trend would reverse itself; that is the waist of the string would grow while the bulge would shrink. Whether this takes place would have to be elucidated by numerical evolutions.

IV. CONCLUSIONS

In the present work we have developed a code based on finite element techniques capable of providing solutions of the constraints describing highly distorted black holes and black strings in spacetimes with arbitrary dimensions D endowed with an $SO(D-2)$ symmetry. We employed such code to investigate a sequence of solutions which contain a marginally trapped surface where both the ADM mass and the asymptotic length of the extra (periodic) dimension are kept fixed. We have concentrated on the $D = 5$ case to make contact with results presented in the literature. (The higher dimensional case is under investigation). The solutions are obtained by providing an arbitrary source (subject to the requirements of the sequence) which can be varied in different regions so as to produce highly distorted black holes and string. Our solutions cover both stable and unstable regimes as far as the the ratio L/M_{ADM} is concerned and the observed behavior is qualitatively similar in both cases.

A study of the sequences obtained reveals several interesting features. First, arbitrary distortions can be obtained

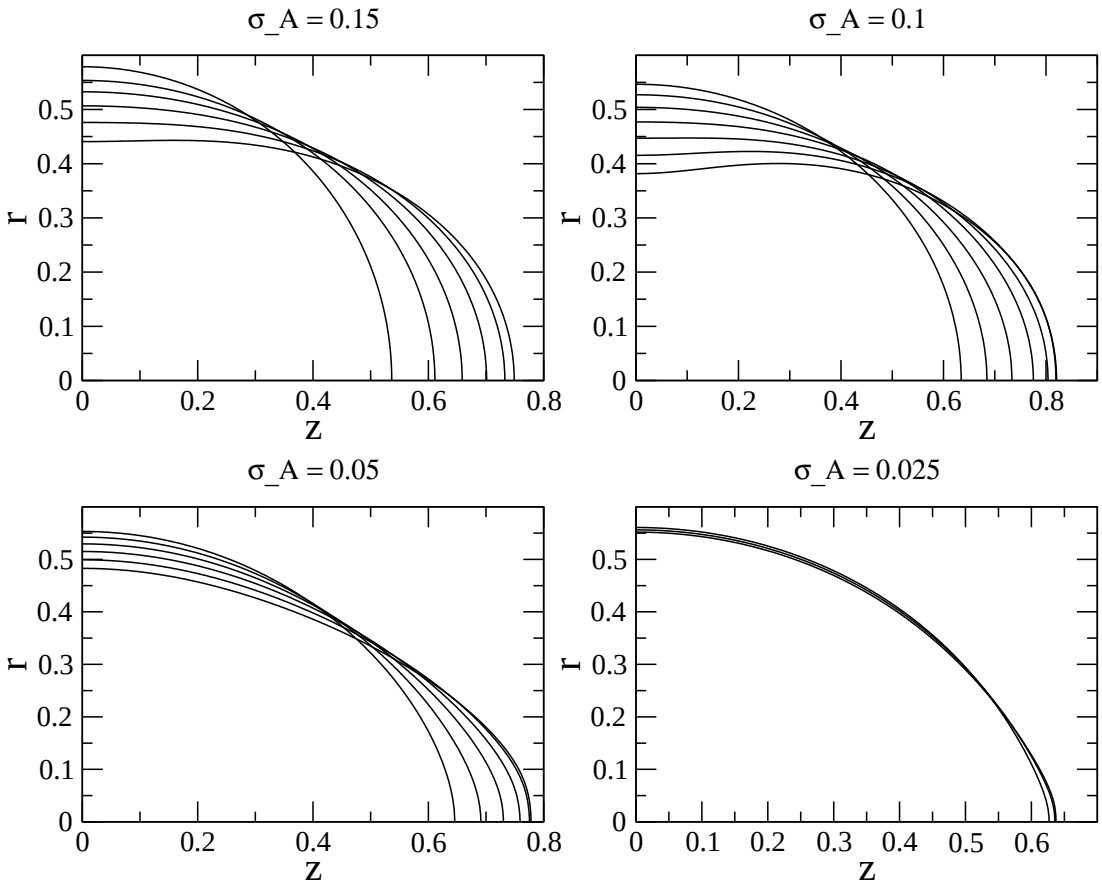

FIG. 2: Distorted black hole horizons all with mass 0.303. The vertical axis is the radial direction, the horizontal axis is the periodic direction. The four sequences of initial data used σ_A values of 0.15, 0.1, 0.05, and 0.025; σ_B values varied from 0.1 to 1.1; σ_r and σ_z were held fixed at 0.1.

both in the black string and black hole phases. Second, even though we can produce arbitrary distorted black holes, the proper distance between the poles seem to have an upper limit in how close these can be made to be as judged by the apparent horizon. Third, we see no evidence of a conical structure developing at or near the waist in the apparent horizon region. The spacetime is smooth in the horizon's vicinity. Note however that the apparent horizon would miss a conical structure at the event horizon unless the spacetime were stationary. Last, the curvature invariant of the apparent horizon corresponding to highly distorted black strings would indicate that the bulge of the horizon approaches a hyperspherical black hole while the neck approaches a black string. Interestingly, this is quite similar to the results obtained at the late stages of the black string simulations presented in [11].

V. ACKNOWLEDGMENTS

This research was supported in part by the NSF under Grants No PHY0244335, PHY0244699, PHY0326311, INT0204937, NASA-NAG5-13430 and funds from the Horace Hearne Jr. Laboratory for Theoretical Physics, CCT-LSU, and a Research Innovation Award from the Research Corporation to Louisiana State University. L. L. was partially supported by the Alfred P. Sloan Foundation.

We wish to thank the Albert Einstein Institute and the National University of Cordoba, Argentina for hospitality at different stages of this work.

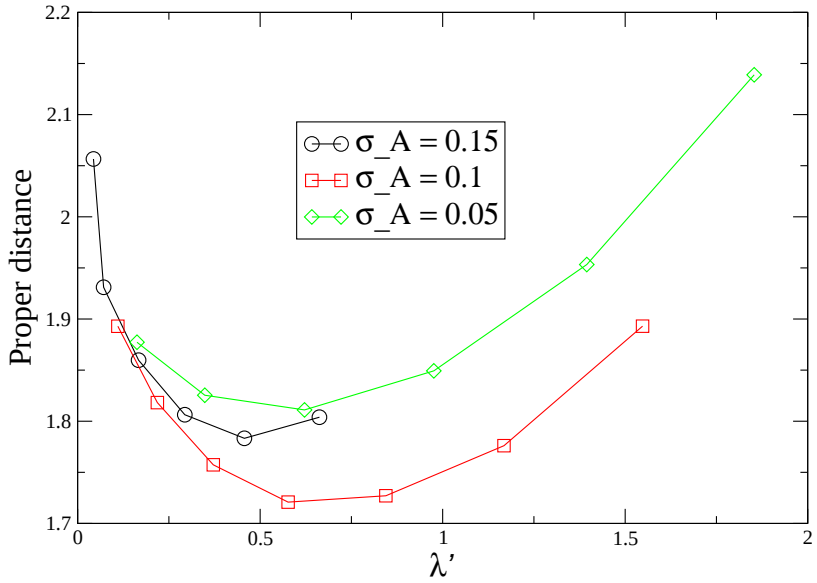

FIG. 3: The proper distance versus black hole distortion, λ' for the data shown in Figure 2.

The authors thank F. Pretorius, O. Sarbach, E. Sorkin and T. Wiseman for discussions.

[1] R. Gregory and R. Laflamme, Phys. Rev. Lett. **70**, 2837 (1993)
[2] R. Gregory and R. Laflamme, "The Instability of charged black strings and p-branes," Nucl. Phys. B **428**, 399 (1994).
[3] G. Horowitz and K. Maeda, Phys. Rev. Lett. **87**, 131301 (2001)
[4] T. Harmark and N. A. Obers, arXiv:hep-th/0503020.
[5] B. Kol, "The phase transition between caged black holes and black strings: A review," arXiv:hep-th/0411240.
[6] S. S. Gubser, Class. Quant. Grav. **19**, 4825 (2002)
[7] T. Wiseman, Class. Quant. Grav. **20**, 1137 (2003)
[8] B. Kol and E. Sorkin, Class. Quant. Grav. **21**, 4793 (2004) [arXiv:gr-qc/0407058].
[9] B. Kol and T. Wiseman, Class. Quant. Grav. **20**, 3493 (2003).
[10] B. Kol, arXiv:hep-th/0206220.
[11] M. Choptuik, L. Lehner, I. Olabarrieta, R. Petryk, F. Pretorius and H. Villegas, Phys. Rev. **D68**, 044001 (2003)
[12] D. Garfinkle, L. Lehner and F. Pretorius, Phys. Rev. D **71**, 064009 (2005)
[13] E. Sorkin and T. Piran, Phys. Rev. Lett. **90**, 171301 (2003).
[14] H. Kudoh and U. Miyamoto, "On non-uniform smeared black branes," arXiv:hep-th/0506019.
[15] E. Sorkin, Phys. Rev. Lett. **93**, 031601 (2004).
[16] J.W. York, in "Sources of Gravitational Radiation" Ed. L. Smarr, Cambridge Univ. Press, New York (1979).
[17] K.-A. Mardal, G. W. Zumbusch, H. P. Langtangen, "Software tools for multigrid methods", in "Advanced topics in computational differential equations: numerical methods and Diffpack programming", H.-P. Langtangen, A. Tveito (editors), Lecture notes in computational science and engineering 33, Springer, New York (2003).
[18] H.-P. Langtangen, "Computational partial differential equations: numerical methods and Diffpack programming (second edition)", Texts in computational science and engineering 1, Springer, New York (2003) http://www.diffpack.com
[19] FlexPDE: http://www.pdesolutions.com/
[20] G. Horowitz, personal communication (2004).

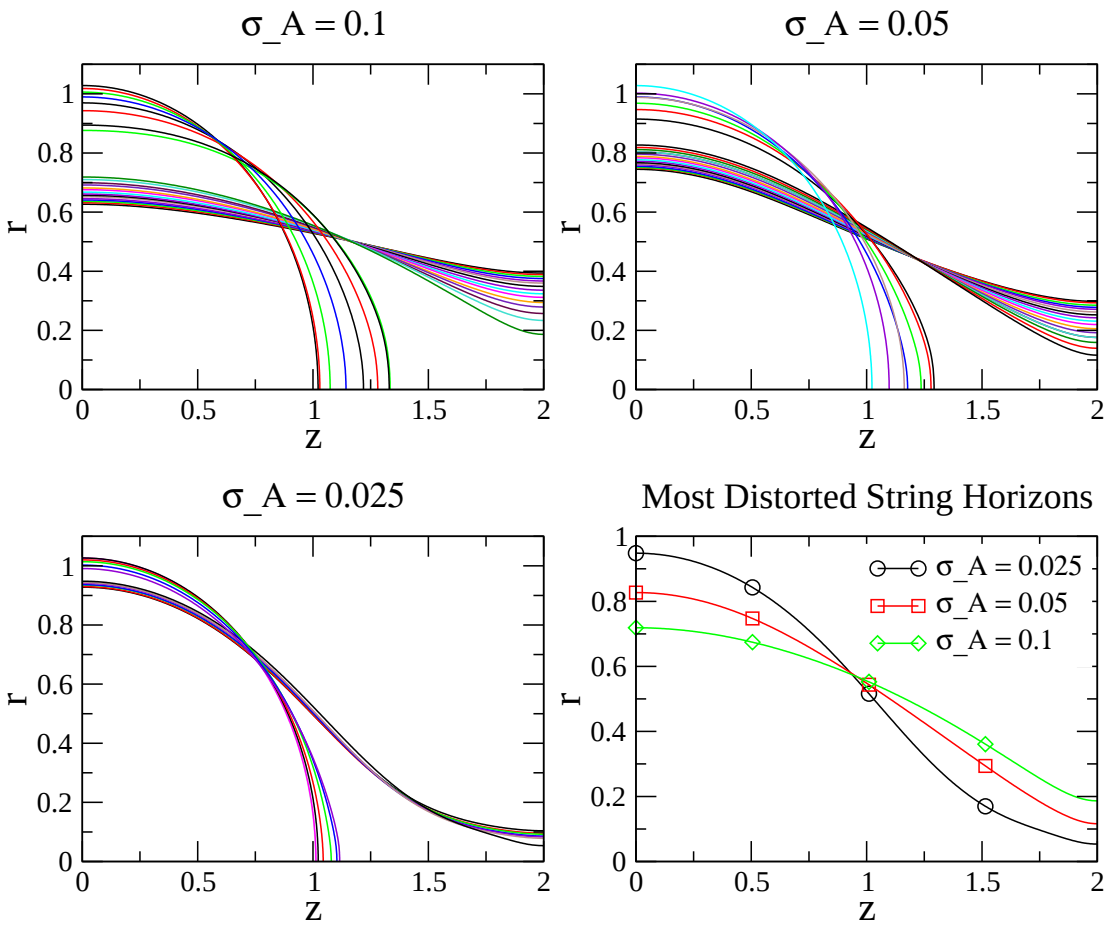

FIG. 4: Distorted black hole and black string horizons. The vertical axis is the radial direction, the horizontal axis is the periodic direction. The three sequences of initial data used σ_A values of 0.1, 0.05, and 0.025; σ_B values varied from 2.0 to 0.1; σ_r and σ_z were held fixed at 0.1. Smaller choices of σ_A produced increasingly distorted black objects. The σ_B value determines whether a string or hole is produced. All data sets had the same ADM mass: 1.52 ± 0.015.

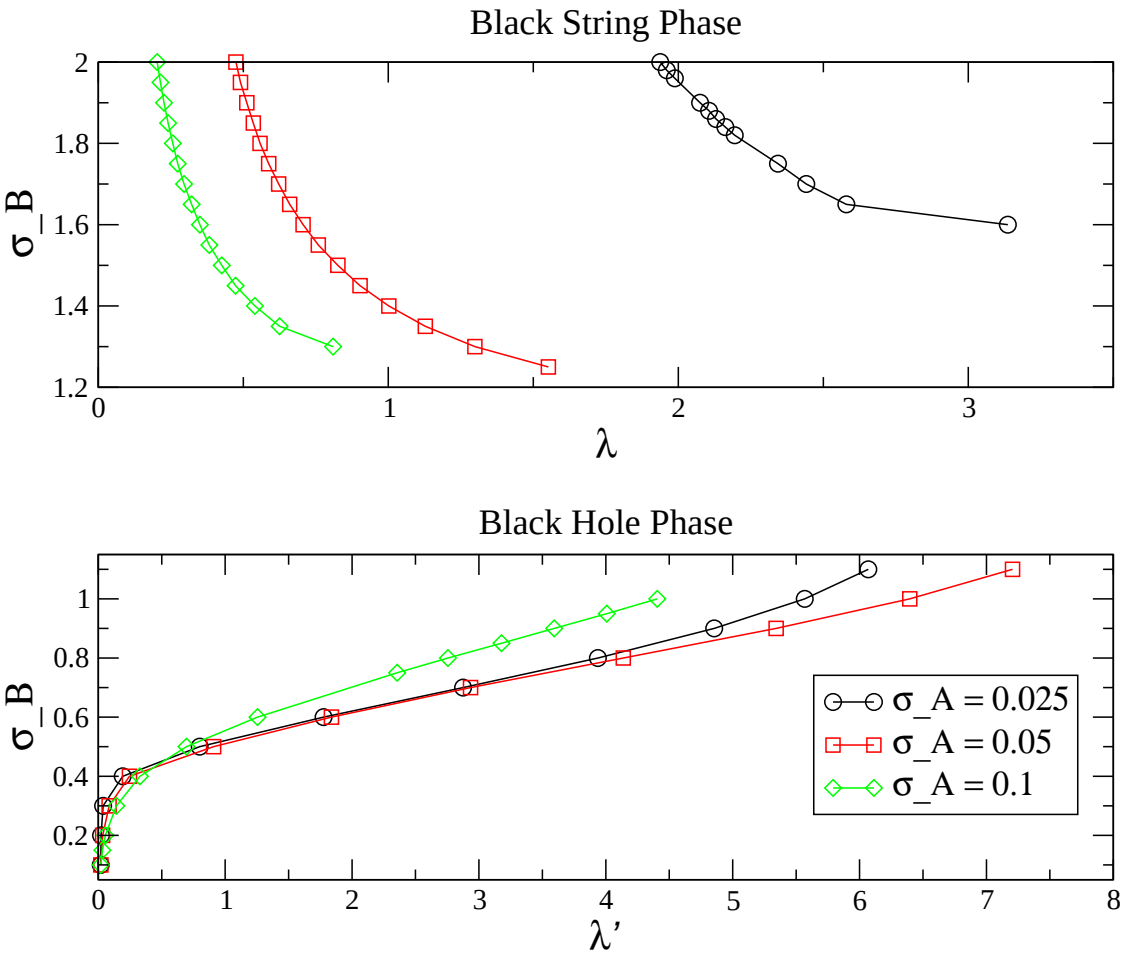

FIG. 5: Top: σ_B vs. black string phase, λ; Bottom: σ_B vs. black hole phase, λ'. Three sets of σ_A values are explored: 0.1, 0.05, and 0.025. All runs had the same ADM mass. As σ_A is decreased, increasingly distorted black string horizons are found. See Figure 4. For $\sigma_A = 0.025$, the horizon finder could not distinguish between a hole or string horizon for σ_B values from 1.5 to 1.2

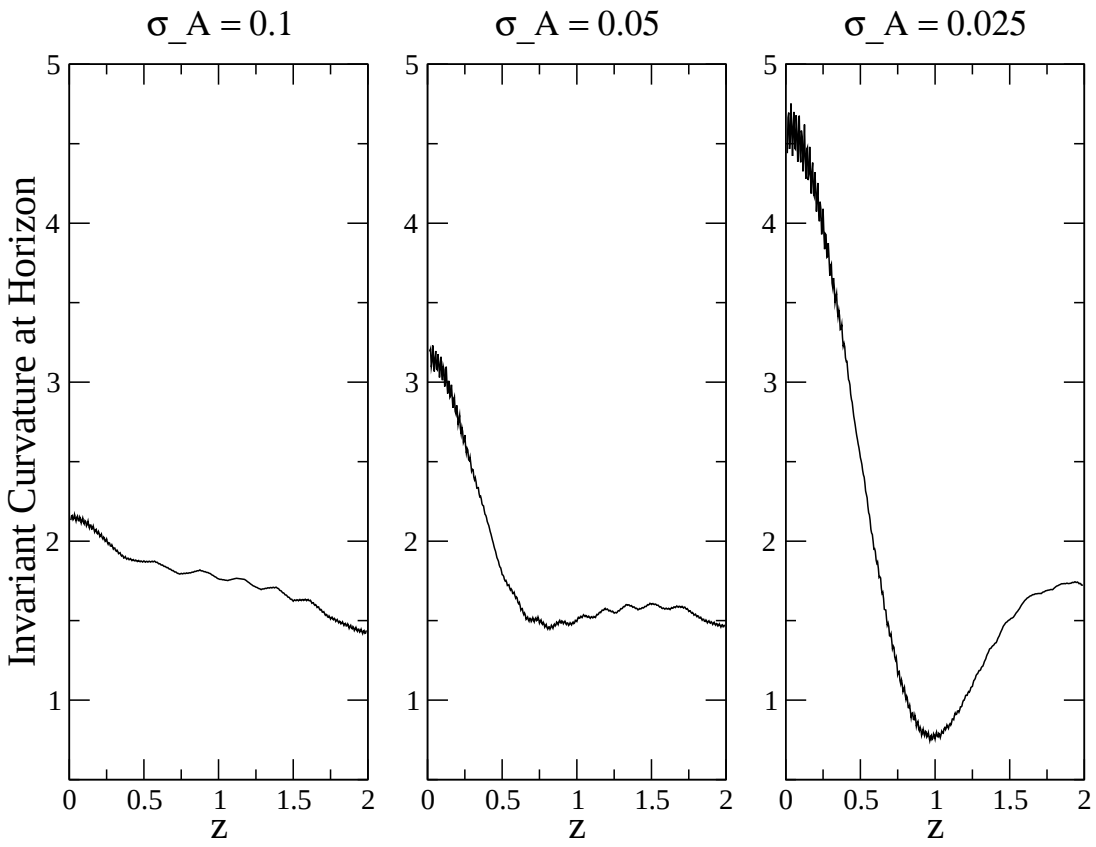

FIG. 6: The invariant curvature at the apparent horizon surface for three sets of distorted black string data using σ_A values of 0.1, 0.05, and 0.025 and a σ_B value of 1.7. All simulations had the same ADM mass. The curvature appears increasingly closer to that for a hyperspherical black hole rather than a black string as the black string is more distorted. See Figures 4, 5.

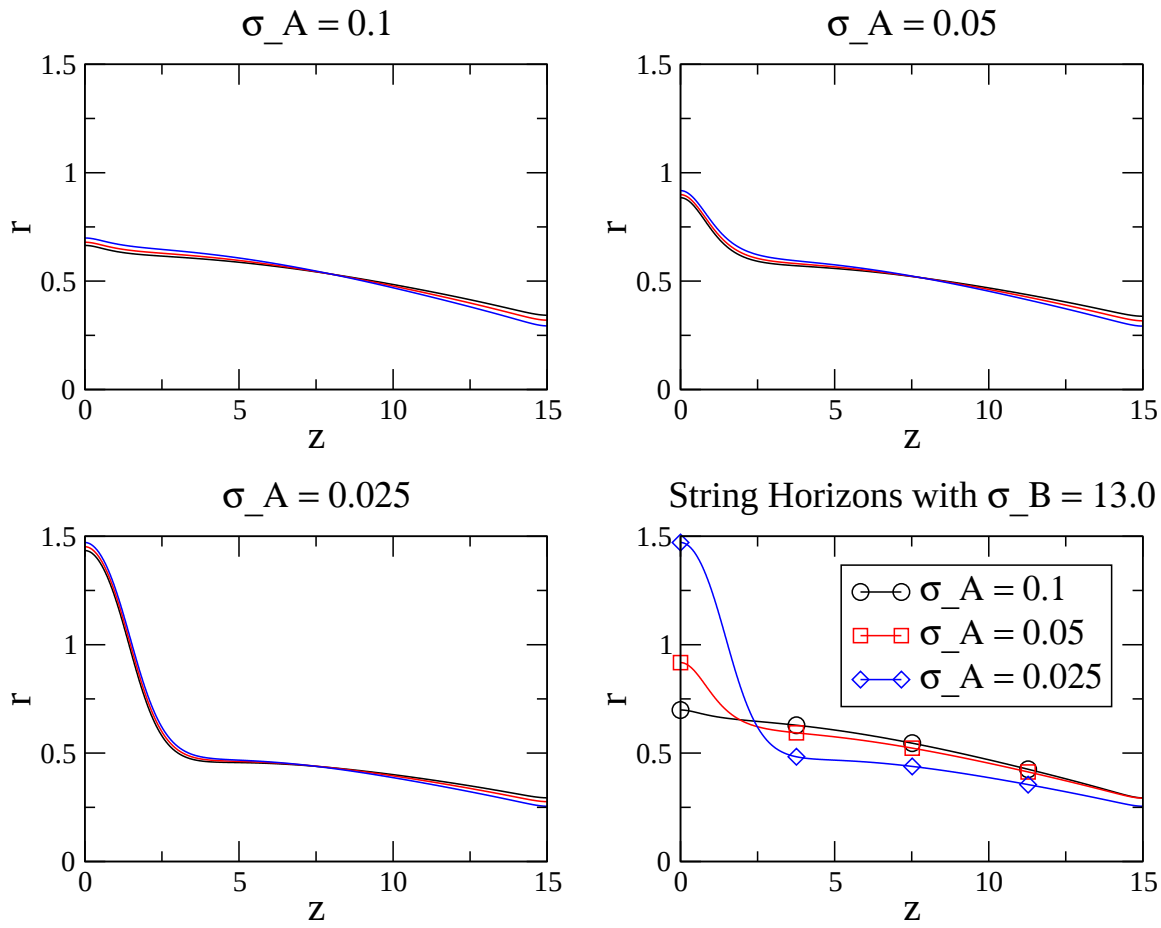

FIG. 7: Distorted black string horizons with $L = 15$ so as to be above the Gregory–Laflamme critical length. The vertical axis is the radial direction, the horizontal axis is the periodic direction. The three sequences of initial data used σ_A values of 0.1, 0.05, and 0.025; σ_B values varied from 15.0 to 13.0; σ_r and σ_z were held fixed at 0.1. All data sets had the same ADM mass: 1.52 ± 0.015. The resolution in these cases was: dr: 0.00225, dz: 0.0145.